

Cooperative Authentication in Underwater Acoustic Sensor Networks

Roe Diamant, Paolo Casari, Stefano Tomasin

Abstract—With the growing use of underwater acoustic communication (UWAC) for both industrial and military operations, there is a need to ensure communication security. A particular challenge is represented by underwater acoustic networks (UWANs), which are often left unattended over long periods of time. Currently, due to physical and performance limitations, UWAC packets rarely include encryption; thus, the UWAN is exposed to external attacks faking legitimate messages. We propose a new algorithm for message authentication in an UWAN setting. We begin by observing that, due to the strong spatial dependency of the underwater acoustic channel, an attacker can mimic the channel associated with the legitimate transmitter only for a single or a small set of receivers. Taking this into account, our scheme is based on the cooperative operation of a set of trusted nodes reporting to a sink node. For each incoming packet, the sink fuses beliefs evaluated by the trusted nodes to reach an authentication decision. These beliefs are based on estimated statistical channel parameters, chosen to be the most sensitive to the transmitter-receiver displacement. Our simulation results show accurate identification of an attacker’s packet. We also report results from a sea experiment demonstrating the effectiveness of our approach.

Index Terms—Underwater acoustic communication, Underwater acoustic communication networks, channel-based security, cooperative security, authentication, UWAC, sea experiment.

I. INTRODUCTION

Underwater acoustic networks (UWANs) are increasingly being perceived as a cost-effective means of ocean exploration and monitoring. While carrying out these tasks, however, UWANs are left unattended over long periods of time, and may become vulnerable to external attacks. The recently introduced standards for underwater acoustic communication [1] make these attacks more probable. For this reason, the investigation of security mechanisms tailored to the specific characteristics of underwater acoustic communications (UWAC) is currently gaining momentum. In particular, it has been observed that only in some specific cases can the same security techniques developed for terrestrial wireless radio networks be directly applicable in underwater scenarios. For example, this is the case of well-known elliptic-curve cryptography schemes, which have been evaluated for underwater applications in [2]. In most other cases, a systematic re-thinking of security schemes and strategies has to be carried out [3]. This fact has spawned a number of solutions exploiting characteristics of UWACs to

achieve resistance against either jamming [4], [5] or denial-of-service (DoS) [6], secure key generation [7] and covert communications [8].

The focus of this paper is the authentication of a packet received by the sink node with the support of the trusted nodes. Authentication mechanisms make it possible for a node to prove that it is a legitimate member of a network, and therefore allow controller nodes or sinks to trust the data sent by the node. This step is of great importance, especially in underwater monitoring tasks and tactical scenarios. The sink’s objective is to determine whether the packet is coming from either the legitimate node or the attacker. Conversely, the attacker’s objective is to let his packet be recognized as authentic by the sink. The authentication is based on the acoustic communication channel’s characteristics, rather than on cryptographic techniques. Trusted nodes support the authentication process, without knowing its outcome, i.e., as the sink collects data from the trusted nodes, it does not broadcast the decision on the authenticity, in order to increase the system’s spectral efficiency and avoid additional security risks.

Our authentication approach is based on channel features that mildly vary over time and space, but are slow enough such that their distribution can be approximated as constant during the authentication process. We choose these parameters by taking an ensemble of data from more than a hundred sea experiments, and by showing that the distributions of channel features –such as the number of channel taps, the delay spread, and the received power level– are all sufficiently constant over time and sufficiently diverse for different transmitter-receiver pairs. This makes such a set of parameters amenable for authentication purposes. For incoming packets received by different trusted nodes, we leverage this diversity by systematically measuring the distribution of the evaluated channel’s characteristics, and by calculating the accumulating clustering belief. The outcome is a measure to discriminate between packets sent by a legitimate transmitter and packets received from intruder nodes. We have tested the performance of our authentication method in both modeled simulations, and in a sea experiment. The results show a good trade-off between the probability of detection and the probability of a false alarm.

The remainder of this paper is organized as follows. Section II surveys the state-of-the-art in UWAC security. Section III describes our system’s model. In Section IV, we discuss our authentication method, and we describe the parameters we use for authentication in Section V. Results from numerical simulations and a sea experiment are shown in Section VI and Section VII, respectively. Conclusions are drawn in Section VIII.

R. Diamant is with the Department of Marine Technology, University of Haifa, Haifa 3498838, Israel (email: roeed@univ.haifa.ac.il).

P. Casari is with the IMDEA Networks Institute, 28198 Madrid, Spain (email: paolo.casari@imdea.org).

S. Tomasin is with the University of Padova, 35131 Padova, Italy (email: tomasin@dei.unipd.it).

II. RELATED WORK

In the following section, we present the literature related to underwater acoustic communication security in general, and to channel-based authentication methods in particular.

A. Underwater Acoustic Communication Security

A comprehensive review of security approaches for underwater networks is provided in [3]. The paper argues that typical wireless network attacks (e.g., sink hole, worm hole, sybil, and black hole attacks) are especially relevant for UWANs deployed in mission-critical or hostile scenarios. After considering several approaches in the literature, each focusing on a different layer of the communication stack, the authors conclude that primary research directions include the prompt detection of malicious nodes, data integrity, as well as computationally simple, energy-efficient and mobility-adaptive secure communication protocols that are possibly designed according to cross-layer principles. The survey in [9] considers a number of similar issues as [3], and proposes software-defined cognitive networks, context-aware routing, cross-layer communications and covert channels as possible solutions to security issues in UWANs.

Jamming is a typical attack in the context of underwater networks. Hence, several approaches focus on modeling and preventing jamming, or on exploiting jamming events to the network's advantage. In [10], [11] simple jamming schemes are tested using typical modems and a prototype orthogonal frequency division multiplexing (OFDM) acoustic modem. It was found that jamming a UWAC is straightforward in many typical scenarios. In [5], it is proposed to model the transmission power in the presence of jamming as a game, for which a Nash equilibrium is found for the case of known channel gains and transmission costs. A different approach is used in [4] to take advantage of jamming by a cooperating node via analog network coding. Using a code division multiple access (CDMA) communication scheme, a data source transmits data to which a cooperative node superimposes its own transmission (known to the source), using the same spreading code as the source itself. Both the cooperating node and the transmission power are optimized in order to guarantee a minimum signal to interference plus noise ratio (SINR) at the receiver, while preventing eavesdropping.

A secure routing protocol for underwater surveillance networks is the target of [6]; the paper also proposes cryptographic primitives (cypher, digest, re-keying) to manage privacy in dynamic networks where nodes may join, leave or be forced to leave when found to be compromised. The network operates based on the flooding of neighbor discovery messages, making the sink aware of the network topology. The sink then runs a Dijkstra algorithm and distributes optimal routes to all nodes. As the flooding protocol may be subject to denial-of-service (DoS) attacks, the protocol is secured by establishing per-link cypher keys.

In [2], the authors evaluate end-to-end authentication through signatures obtained via the elliptic curve digital signature algorithm (ECDSA), the Zhang-Safavi-Naini-Susilo (ZSS) algorithm, which has been shown to be computationally

efficient in resource-constrained platforms, and the Boneh-Lynn-Shacham (BLS) algorithm, which can generate aggregate signatures.

A robust key generation scheme is proposed in [7]. The approach processes channel characteristics through fuzzy information reconciliation, which flattens the differences in the typically asymmetric two-way channels encountered in underwater communications (which are generally much less stable than their terrestrial radio counterparts (see for instance the channel-based authentication scheme in [12])). The approach in [7] makes it more difficult for an eavesdropper, who would perceive a different channel response, to generate the same key as the legitimate network nodes.

Covert communications are considered an inherent security mechanism in [8], which proposes a OFDM scheme, achieving either 4.2 or 78 bit/s over a bandwidth of 3.6 kHz. The scheme can successfully pick up signals, even at low signal-to-noise ratios (SNRs) and in the presence of severe delay and Doppler spread conditions. The multiband OFDM modulation scheme in [8] becomes vulnerable only if the attacker identifies the spreading code employed in the signal. Direct-sequence spread spectrum (DSSS) has been used to provide covert communications [13], [14], but a recent work [15] has shown that the spreading code can be blindly identified by an attacker who has no channel state information and is oblivious of the training sequence used. This is also one part of the rationale behind the cooperative jamming approach in [4]. In [16], we have outlined theoretical bounds to measure the performance of covert UWAC as a function of the communication parameters and the channel parameters, and show that covertness improves for slower transmissions in shallower waters.

B. Methods for Channel-based Authentication

User authentication has been addressed by the so-called physical layer security by exploiting the channel coherence, i.e., messages going from the same source to the same destination undergo the same channel, whereas a message coming from a fake source located in a different position will be subject to a different channel, which can be estimated at the destination. This approach has been applied in a variety of scenarios, especially in a radio wireless context (see [17] for a survey). Typically, channel-based authentication is based on the comparison of one reference channel estimate (obtained using a different authentication method) with the current channel estimate; in order to take into account channel variations due to fading and shadowing, the reference estimate can be updated based on the next received authenticated messages [18]. Various channel features have been considered in the context of performing authentication. For example, in a wireless radio context, the power level was considered in [19]–[21], the impulse response of a wideband channel in [22]–[26], the frequency response of an OFDM transmission in [27], and the power spectral densities in [28]. When multiple nodes are available, the authentication process can be further enhanced.

In [12], a distributed authentication in wireless networks was considered where multiple sensors report their correlated measurements to a fusion center, which makes the ultimate

authentication decision, and scheduling of sensor cooperation is performed, taking energy constraints into account. In [29], a similar solution using compressed sensing is studied. All these works typically assume a given channel statistic, which is used to formulate the authentication hypothesis testing problem. In [30], this assumption is removed by using logistic regression techniques, which is applied to the received power signal.

III. SYSTEM MODEL

We consider an underwater acoustic network with a sink node assisted by N trusted nodes, one legitimate transmitter, and one attacker. Extension to deployments consisting of multiple nodes is straightforward. Transmissions are organized in packets of T symbols. We assume that the first set of received packets (e.g., the first packet) always comes from the legitimate node. Then, the following packets can arrive from the legitimate transmitter or from the eavesdropper. Each transmitted packet is labeled with a unique identification (ID) number that prevents replay attacks. Moreover, trusted nodes are assumed to be roughly time-synchronized with a resolution corresponding to the expected transmission rate of the packets by the legitimate transmitter, and the channel's propagation delay. That is, we assume that the times at which the trusted node receives a packet with a specific ID (according to their own clock) are within a reasonable time span. This prevents the retransmission of the same packet by the attacker with beamforming/channel modification techniques aimed at passing the authentication procedure.

A. Assumptions about the Channel's Features

In the UWAC channel, the transmitted signal is reflected from both the sea boundaries and volume scatterers, such as plankton and sediments. Moreover, due to the continual motion of the waves, signals are affected by a Doppler shift varying up to tens of Hz [31]. The channel is characterized by a tapped delay line, whose delay spread is in the order of hundreds of taps [32], significant variations for different transmitter-receiver locations. The power attenuation of the UWAC channel is governed by the propagation loss and the absorption loss. The propagation loss is a function of the channel structure and entails a highly non-linear process [33], which creates both convergence zones where the acoustic signal is clearly received, and shadow zones where the signal is significantly attenuated [34]. Moreover, the sound propagation between layers, characterized by different sound speeds (mostly due to water pressure or temperature changes), leads to both refractions and additional attenuation [35]. The absorption loss is a function of the carrier frequency, and is mainly affected by water temperature, salinity, and pressure [35]. Since propagation and absorption losses cannot be separated at the receiver, we use the overall attenuation level.

Our proposed authentication method relies on features extracted from the underwater acoustic channel, such as the number of channel taps, the channel's delay spread, and the received power level. These features are assumed to be location-dependent such that the channel realization observed by a trusted node for packets received from the legitimate

node is different than that of an attacker located far from the legitimate node. Even if underwater channels are typically time-varying, we assume that the statistics of the features do not change, as long as the transmitter and receiver locations remain relatively stable. Later, we will validate this assumption based on more than 100 sea experiments conducted at various times and in diverse environments over a four-year period.

Let $x_{i,n}(t)$ be the i th, $i \in [1, I]$, estimated channel feature extracted at time $t \in \mathcal{T}_\phi$ at trusted node $n \in [1, N]$, where \mathcal{T}_ϕ is the set of times in which packet ϕ has been received. We model the conditional probability density function (PDF) of $x_{i,n}(t)$ as the general Gaussian [36]

$$p_{x|\omega}(a|\omega_{i,n}) = \frac{\beta_{i,n}}{2\sigma_{i,n}\Gamma\left(\frac{1}{\beta_{i,n}}\right)} e^{-\left(\frac{|a-\mu_{i,n}|}{\sigma_{i,n}}\right)^{\beta_{i,n}}}, \quad (1)$$

which is identified by the set of parameters

$$\omega_{i,n} = (\beta_{i,n}, \sigma_{i,n}, \mu_{i,n}). \quad (2)$$

Distribution (1) is chosen to provide flexibility. In particular, by choosing parameter $\beta_{i,n}$, we obtain the Laplace distribution ($\beta_{i,n} = 1$), the Gaussian distribution ($\beta_{i,n} = 2$) and the uniform distribution ($\beta_{i,n} \rightarrow \infty$). On the other hand, $\mu_{i,n}$ is the average of the estimation (which approaches the true value), and $\sigma_{i,n}$ is related to the estimation variance. Note that we assume the feature statistics $\omega_{i,n}$ are static, i.e., they do not change over time, not even across different packets. The validity of this assumption is proven through a sea experiment, as described in Section VII.

B. Assumptions on the Attacker Model

We assume that the attacker is a single malicious node, able to perform any kind of signal processing on its transmitted packet. In particular, it has unlimited power transmission capabilities, it can filter the transmitted signal in order to let the trusted node estimate a different channel, and it can superimpose signals onto the message. We also assume that the attacker knows:

- 1) the position of both the trusted nodes and the legitimate node;
- 2) the training signals used for channel estimation by the trusted nodes;
- 3) the statistical correlation of its channels to each trusted node/legitimate node with the channels between the legitimate node and the trusted nodes;
- 4) the instantaneous channels from itself to both the legitimate node and the trusted nodes.

IV. AUTHENTICATION METHOD

In this section, we outline the details of our authentication method. Our user authentication scheme aims at establishing the authenticity of a received packet. This is a hypothesis-testing problem, where for a packet ϕ , the two hypotheses are

- \mathcal{H}_0 : packet ϕ is authentic and
- \mathcal{H}_1 : packet ϕ is not authentic.

false alarm (FA) reflects the case in which an authentic packet is classified as not authentic; missed detection (MD)

reflects the case in which a non-authentic packet is classified as authentic. For a given testing strategy, the FA and MD probabilities are the probabilities that a FA or a MD occur.

Our authentication is based on the set of estimated parameters $\mathbf{X}(\phi) = \{x_{i,n}(t), t \in \mathcal{T}_\phi, \forall i, n\}$ associated with packet ϕ . Let $p_{\mathbf{X}|\mathcal{H}}(\mathbf{X}(\phi)|\mathcal{H}_m)$ be the joint PDF of $\mathbf{X}(\phi)$ conditional upon hypothesis \mathcal{H}_m . Then, for packet ϕ , the optimal hypothesis testing strategy is obtained by computing the log-likelihood ratio (LLR) [37]

$$\Psi_\phi = \Psi_\phi^0 - \Psi_\phi^1, \quad (3)$$

where

$$\Psi_\phi^m = \log p_{\mathbf{X}|\mathcal{H}}(\mathbf{X}(\phi)|\mathcal{H}_m), \quad m = 0, 1. \quad (4)$$

The decision procedure for the hypothesis testing problem therefore becomes

$$\hat{\mathcal{H}} = \begin{cases} \mathcal{H}_0 & \Psi_\phi < \lambda, \\ \mathcal{H}_1 & \Psi_\phi \geq \lambda, \end{cases} \quad (5)$$

where λ is a threshold that trades off between the FA and MD probabilities.

A. Distributed Authentication

Our authentication method is distributed in the sense that each trusted node performs a pre-processing procedure on the received packet to reduce the amount of data to be exchanged with the sink node which, in turn, will determine the authenticity of each packet. In the following, we derive both the data provided by the trusted nodes and the fusion procedure at the sink.

We consider (1) as the PDF of the channel features used for authentication; however, we do not know the parameters $\omega_{i,n}^m$ a-priori. Instead, we estimate $\omega_{i,n}^m$ using all received packets up to packet ϕ , and we indicate this estimate as $\hat{\omega}_{i,n}^m(\phi) = (\hat{\beta}_{i,n}^m(\phi), \hat{\sigma}_{i,n}^m(\phi), \hat{\mu}_{i,n}^m(\phi))$. We use the estimated parameters to compute the conditional probability, such that, assuming that the errors affecting the parameter estimates are independent and identically distributed (iid), we have

$$p_{\mathbf{X}|\mathcal{H}}(\mathbf{X}(\phi)|\mathcal{H}_m) = \prod_{i,n,\tau \in \mathcal{T}_\phi} p_{x|\omega}(x_{i,n}(\tau)|\hat{\omega}_{i,n}^m(\phi)), \quad m = 0, 1, \quad (6)$$

where $m = 1$ and $m = 2$ denote the classification of “legitimate” and “fake,” respectively.

The details about the estimate of the parameters $\hat{\omega}_{i,n}^m(\phi)$ are provided in the next subsections. Plugging (6) in (4), the LLR (3) is written as

$$\Psi_\phi = \sum_n R_{\phi,n} \quad (7)$$

where

$$R_{\phi,n} = \Psi_{\phi,n}^0 - \Psi_{\phi,n}^1, \quad (8)$$

$$\Psi_{\phi,n}^m = \sum_{i,\tau \in \mathcal{T}_\phi} \log \frac{\hat{\beta}_{i,n}^m(\phi)}{2\hat{\sigma}_{i,n}^m(\phi)\Gamma\left(\frac{1}{\hat{\beta}_{i,n}^m(\phi)}\right)} \times e^{-\left(\frac{|x_{i,n}(\tau) - \hat{\mu}_{i,n}^m(\phi)|}{\hat{\sigma}_{i,n}^m(\phi)}\right)^{\hat{\beta}_{i,n}^m(\phi)}}. \quad (9)$$

From (7)–(9), we observe that the computation of the LLR can be split among the N trusted nodes: each trusted node estimates the parameter set $\hat{\omega}_{i,n}^m(\phi)$, computes the two LLRs for $m = 0, 1$, and forwards $R_{\phi,n}$ to the sink. Then, at the sink, (7) is used to compute the packet LLR.

B. Estimation of the PDF Parameters at the Trusted Nodes

As mentioned above, in order to compute (7) and (8), each trusted node n must estimate the set of PDF parameters, $\hat{\omega}_{i,n}^m(\phi)$, for the two hypotheses $m = 0$ and $m = 1$. Note that although no prior information on packet authenticity is initially available to the trusted nodes, one possibility to classify the packets as authentic or not authentic entails the use of the decision on the hypothesis testing problem at the sink. This would require feeding the decision outcome from the sink back to the trusted nodes, a process that increases the authentication procedure’s overhead, and which must also be secured against further attacks (e.g., forging or jamming attacks on the feedback packet). Here, we do not employ any feedback, but rather propose a technique by which each trusted node estimates all parameters and associates them with the two hypotheses.

Parameter Estimation — As the estimation criterion, we consider the maximum likelihood approach, in which parameters are selected in order to maximize the probability of the observations. Given the parameters, we employ the mixture model

$$\begin{aligned} \mathbb{P}(X_{i,n}(\phi)|\hat{\omega}_{i,n}^0(\phi), \hat{\omega}_{i,n}^1(\phi)) &= \\ &= \prod_{t \in \mathcal{T}_\phi} \sum_{m=0}^1 k_{i,n}^m p_{x|\omega}(x_{i,n}(t)|\hat{\omega}_{i,n}^m(\phi)), \end{aligned} \quad (10)$$

where $X_{i,n}(\phi) = \{x_{i,n}(t), t \in T_f, f \leq \phi\}$ (i.e., we use all observations collected so far), and $k_{i,n}^m$ is the prior on parameter i at node n about hypothesis m (which is also unknown and must be estimated). We let each trusted node estimate the set $\theta_{i,n}^m = (\omega_{i,n}^m, k_{i,n}^m)$.

Let us now define the set $\Theta_{i,n} = \{\theta_{i,n}^m, m = 0, 1\}$ and similarly the corresponding set of estimated parameters at packet ϕ as $\hat{\Theta}_{i,n}(\phi)$. Note that $\theta_{i,n}^m$ is not packet-dependent, in accordance with our assumption that the feature statistics for both the legitimate and the attacker do not change much for different packets. However, its estimate, $\hat{\theta}_{i,n}^m(\phi)$, is updated at each packet. The estimated parameters $\hat{\Theta}_{i,n}(\phi)$ maximize the likelihood of observing $X_{i,n}(\phi)$. That is, taking into account the fact that observations $x_{i,n}(t)$ are independent for different t (even when belonging to the same packet),

$$\hat{\Theta}_{i,n}(\phi) = \operatorname{argmax}_{\Theta = (\omega_{i,n}^m, k_{i,n}^m)} \mathbb{P}(X_{i,n}(\phi)|\Theta_{i,n} = \Theta). \quad (11)$$

We find the solution of the maximization problem (11) via the expectation maximization (EM) algorithm [37], as detailed in the Appendix.

Parameter Association — The EM algorithm provides the estimated parameter sets $\hat{\theta}_{i,n}^m$, for $m = 0$ and $m = 1$. However, without further information about the expected values for each of the two classes $m = \{0, 1\}$, the association of $\hat{\theta}_{i,n}^m$ to hypothesis \mathcal{H}_0 and \mathcal{H}_1 is ambiguous. In other words, we do

not know if $m = 0$ is actually associated with hypothesis \mathcal{H}_0 or hypothesis \mathcal{H}_1 . Therefore, when fusing all data at the sink, we must synchronize m across the trusted nodes to ensure that the same value of m refers to the same hypothesis for all the trusted nodes.

In order to remove this ambiguity, according to our assumption that the first packet always originates from the legitimate transmitter, we let all trusted nodes assign hypothesis $m = 0$ to the first packet with index $\phi = 0$. Then, the labeling m is chosen by matching the current estimated variables $\hat{\theta}_{i,n}^m$ to the measurements from the first packet, $\mathcal{X}_{i,n}(0)$. Formally, we associate $\hat{\theta}_{i,n}^0(\phi)$ with hypothesis \mathcal{H}_0 if

$$\mathbb{P}(\mathcal{X}_{i,n}(0)|\hat{\theta}_{i,n}^0(\phi)) \geq \mathbb{P}(\mathcal{X}_{i,n}(0)|\hat{\theta}_{i,n}^1(\phi)), \quad (12)$$

and from (1), condition (12) becomes

$$\prod_{t \in \mathcal{T}_0} p_{x|\omega}(x_{i,n}(t)|\hat{\omega}_{i,n}^0(\phi)) \geq \prod_{t \in \mathcal{T}_0} p_{x|\omega}(x_{i,n}(t)|\hat{\omega}_{i,n}^1(\phi)). \quad (13)$$

After this association procedure, for $m = 0$, trusted node n calculates (9) and from it the decision index $R_{\phi,n}$ in (10), according to the $\hat{\theta}_{i,n}^m$, which was associated with hypothesis \mathcal{H}_0 , and vice versa for the $\hat{\theta}_{i,n}^m$, which was associated with hypothesis \mathcal{H}_1 .

C. Refined Data Fusion

We observe that in the above distributed procedure, two possible errors may arise: a) a hypothesis association error, and b) a parameter estimation error. The first error arises when m is assigned different values for the same hypothesis by different nodes. This occurs when test (12) fails. To resolve this issue, since the sink node obtains more information than each trusted node, we let the sink correct this type of incorrect assignment by simply flipping the sign of the reported data $R_{\phi,n}$. The second error arises when the observed data is noisy and does not represent the full parameter statistics, or when the attacker manages to confuse a trusted node. In this case, the sink node can improve the data fusion by weighting the reported values $R_{\phi,n}$. The two refinements are obtained by replacing (7) with

$$\Psi_\phi = \sum_n g_n(\phi) s_n(\phi) R_{\phi,n}, \quad (14)$$

where $s_n(\phi) \in \{-1, 1\}$ is the binary correction factor for the hypothesis association, and $g_n(\phi) > 0$ is a weight to correct PDF parameter estimation errors.

Choice of $s_n(\phi)$ — In this case, we propose choosing s_n at the sink node, so as to maximize the agreement among the trusted nodes. Formally, the set $\mathbf{s}(\phi) = \{s_1(\phi), \dots, s_N(\phi)\}$ is chosen as

$$\mathbf{s}(\phi) = \operatorname{argmax}_{\hat{s}_n \in \{-1, 1\}^N} \left| \sum_n \hat{s}_n R_{\phi,n} \right|, \quad (15)$$

so that the best agreement among the trusted nodes is reached. *Choice of $g_n(\phi)$* — The weighting mechanism reflects the fact that the physical location of the trusted node matters. In particular, the parameter evaluation improves if the trusted node is closer to the packet source, be it the legitimate transmitter or the attacker. Moreover, regarding the possibility

that the attacker imitates a certain transmitter-trusted node channel, we observe that a better decision is made if the trusted nodes are spread around the network area, instead of being clustered close to one another. This is because for each false packet sent, the attacker (in the event there is one) can only mimic the channel efficiently in a specific area.

We use channel parameter i^* as a measure of closeness to the packet source.¹ Taking the above considerations into account, after [38] we formalize the weighing function to be

$$g_n(\phi) = \left(\frac{\bar{x}_{i^*,n}(\phi)}{\max_{n'}(\bar{x}_{i^*,n'}(\phi))} \right)^{-2} (1 + \zeta_n), \quad (16)$$

where $\bar{x}_{i^*,n}(\phi)$ is the mean (or median) of the set $\{x_{i^*,n}(t), t \in \mathcal{T}_\phi\}$. Parameter ζ_n is a measure of how much a trusted node n is isolated, and we use

$$\zeta_n = \sum_{k \neq n} \zeta_{n,k}, \quad (17)$$

where

$$\zeta_{n,k} = \frac{1}{\sum_{j \neq k,n} \bar{x}_{i^*,j}(\phi)} \sum_{j \neq k,n} \frac{1}{\bar{x}_{i^*,j}(\phi)} \times \left(1 - \frac{(\mathbf{p}(k) - \mathbf{p}(n))^T (\mathbf{p}(j) - \mathbf{p}(n))}{\bar{x}_{i^*,n}(\phi) \bar{x}_{i^*,k}(\phi)} \right) \quad (18)$$

is a normalized distribution measure between nodes n and k , and $\mathbf{p}(\ell)$ is the set of UTM coordinates of node ℓ , such that isolated trusted nodes receive a higher weight.

Algorithm 1 summarizes the proposed authentication procedure. The algorithm is performed first by the trusted nodes (lines 3-7), and then by the sink (lines 9-16). Then, the decision is made by the sink (lines 12-16).

V. PARAMETERS FOR PHYSICAL LAYER AUTHENTICATION

The key features used to determine the integrity of an underwater acoustic transmission are the number of channel taps, the tap power, the coherence time, the root mean square (RMS) of the relative delay experienced by the channel taps with respect to the first tap, and a smoothed version of the received power. The effectiveness of the authentication features is provided by the fact that they are relatively stable over time, so their distribution can be approximated as static, but varying considerably in space, so that an attacker located in a different position can be distinguished from the authentic transmitter. In this section, we discuss the rationale behind our choice of channel features.

A. Definition of Channel Features used for Authentication

Consider a measured channel impulse response $h_n(t, \tau)$ for time t , delay τ , and node n , for $0 \leq \tau \leq L_n(t)$, where $L_n(t)$ is the total number of taps at time t , and we call the set of these taps $\mathcal{L}_n(t)$, i.e., $L_n(t) = |\mathcal{L}_n(t)|$. The following channel features are considered for authentication by trusted node n :

¹In our analysis, we consider this parameter to be the received power level. Given the presentation of the channel features to be used for authentication in Section V-A, this corresponds to $i^* = 6$.

Algorithm 1 Cooperative Authentication Algorithm

Require: Set of channel measurements $\{x_{i,n}(t), t \in \mathcal{T}_\phi\}$, $i = 1, \dots, 4$,
 \forall trusted node n , \forall current and previous packets ϕ ;

Ensure: Authentication decision for a packet ϕ ;

Begin

```

1: Calculate  $\omega_{i,n}^m$ ,  $m = 0, 1$  (see Section V);
2: for each received packet  $\phi$  do
3:   for each trusted node  $n$  do
4:     At trusted node  $n$ :
5:     Associate hypothesis  $m = \{0, 1\}$  by (13);
6:     Calculate  $\Psi_{\phi,n}^m$  from (9);
7:     Calculate local decision index  $R_{\phi,n}$  by (8);
8:     Forward  $R_{\phi,n}$  to sink;
9:   end for
10:  At the sink:
11:  Calculate hypothesis correction  $s_n$  by (15);
12:  Calculate trusted nodes' weights  $g_n$  by (16);
13:  Calculate decision index  $\Psi_\phi$  by (14);
14:  if  $\Psi_\phi \geq \lambda$  then
15:    packet is authentic;
16:  else
17:    packet is false;
18:  end if
19: end for

```

End

1—Number of channel taps. Defining the set $\mathcal{S}_n(t) = \{\tau : |h_n(t, \tau)| > T_h\}$, where T_h is a threshold (see [39] for details), the estimated number of significant taps is

$$x_{1,n}(t) = |\mathcal{S}_n(t)|. \quad (19)$$

2—Tap Power. We measure the average tap power as

$$x_{2,n}(t) = \frac{1}{|\mathcal{S}_n(t)|} \sum_{\tau \in \mathcal{S}_n(t)} h_n(t, \tau). \quad (20)$$

3—Coherence Time. The coherence time conveys the duration of time which the channel remains roughly the same. Formally, we define

$$x_{3,n}(t) = \operatorname{argmax}(\Delta) \text{ s.t. } \operatorname{NC}(h_n(t, \tau), h_n(t - \Delta, \tau)) > 0.9, \quad (21)$$

where $\operatorname{NC}(\alpha, \beta)$ is the normalized correlation between α and β .

4—RMS delay spread. Assuming that the arrival delay of each channel tap is measured in relation to the delay of the first tap, the estimate of the RMS delay spread is computed as

$$x_{4,n}(t) = \sum_{\tau \in \mathcal{L}_n(t)} (\tau - \bar{\tau})^2, \quad (22)$$

where $\bar{\tau} = \frac{1}{|\mathcal{L}_n(t)|} \sum_{\tau \in \mathcal{L}_n(t)} \tau = \frac{L_n(t)(L_n(t)+1)}{2}$.

5—Average path delay. The average path arrival time, relative to the arrival of the first tap, is

$$x_{5,n}(t) = \frac{1}{|\mathcal{S}_n(t)|} \sum_{\tau \in \mathcal{S}_n(t)} \tau. \quad (23)$$

6—Received power level. Since we expect the received level to change, we consider the difference between the current power measurement and a smoothed version of previous measurements. Formally, let $q_{n,t}$ be the power of a symbol

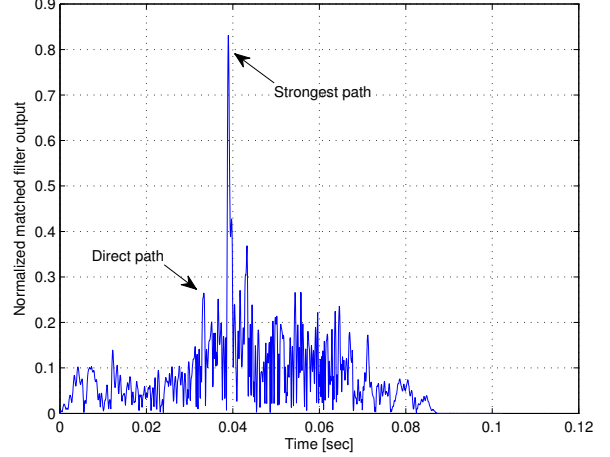


Fig. 1. Example of an impulse response from the database in [40]

received at time t by node n . The smoothed power with a power measurement at a previous time t' is defined by

$$x_{6,n}(t) = \alpha \cdot q_{n,t} + (1 - \alpha) \cdot \tilde{q}_{n,t'}, \quad (24)$$

where α is a user-defined parameter, and t' is the time when the previous feature measurement was performed.

Other channel features can also be used for authentication. For example, the Doppler shift would be a good candidate, since it inherently changes for different transmitter/receiver locations. However, marked differences in Doppler shift require one or more of the network nodes to move. In order to make our authentication procedure as general as possible, we do not include Doppler shift as an authentication feature. Similarly, the time of arrival of a packet transmission would also be a good channel feature for authentication purposes. However, since the trusted node would need to cooperate with the transmitter in order to determine the transmission time, the time of arrival is more vulnerable to attacks, and therefore we avoid using it.

B. Statistical Analysis of the Channel Features

In order to assess the sensitivity of the channel features to the transmitter and receiver locations, we performed a statistical analysis using time-based channel impulse responses recorded during more than 100 sea experiments of different water depths, seasons, and locations. All experiments were performed along the Israeli coast between 2001-2005, and included the use of various acoustic equipment at different carrier frequencies. The channels were recorded for at least 10 s with a resolution of 50 ms. The database format is reported in [40]. An example of an impulse response acquired from this database is shown in Fig. 1.

From the database in [40], we selected the experiments that included more than two nodes, so that we could compare the differences between the considered channel features in space at the same time. To capture fluctuations due to environmental changes on a small time scale, this comparison is performed

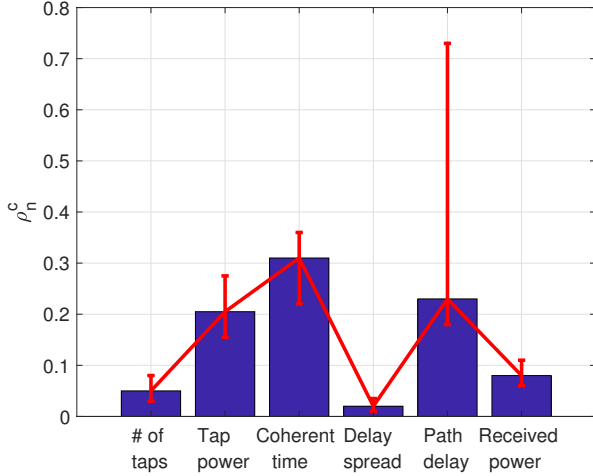


Fig. 2. Average ρ^c from (25) for spatial and time dependency of some acoustic channel features.

for the time series rather than for average values. As the receivers used similar hydrophones for reception, in this section we drop the node index n from the notation.

For the same transmitter and a pair of receivers i and j within the set of receiver pairs \mathcal{R} in the same sea experiment, we evaluate the difference between the time series of the estimated channel features \mathbf{x}_j and \mathbf{x}_i with elements $x_j(t)$ and $x_i(t)$, respectively, obtained at the same time instances $t = 0, \dots, T_N - 1$. The difference between the two time series provides a measure of the spatial dependency of the estimated feature. Yet, to be used as authentication measures, the chosen features must also not change significantly during the acquisition time. As a metric for the comparison, we used

$$\rho^c = \frac{1}{|\mathcal{R}|} \sum_{(i,j) \in \mathcal{R}, r \neq d} \frac{\sum_{t=0}^{T_N-1} x_j(t)x_i(t)}{\sqrt{\sum_{t=0}^{T_N-1} x_j^2(t) \sum_{t=0}^{T_N-1} x_i^2(t)}} \times (1 - \rho^{\text{diff}}(\mathbf{x}_j)) (1 - \rho^{\text{diff}}(\mathbf{x}_i)), \quad (25)$$

where $|\cdot|$ is the rank of \cdot , and $\rho^{\text{diff}}(\mathbf{x}_j)$ is the Jain's fairness index [41]

$$\rho^{\text{diff}}(\mathbf{x}_j) = \frac{\left(\sum_{t=0}^{T_N-1} x_j(t) \right)^2}{T_N \sum_{t=0}^{T_N-1} x_j^2(t)}, \quad (26)$$

used to estimate the variation of the considered channel feature over time. Note that metric ρ^c decreases, the more spatially dependent but time independent the channel feature is. Hence, to authenticate transmissions, we prefer features with small ρ^c .

Fig. 2 shows the average ρ^c for the different considered measured channel features in Section V-A. All features were measured by estimating the channel impulse response over time (see full description in [40]), and by processing it to extract the feature values. While there is a considerable difference between other features estimated at different locations,

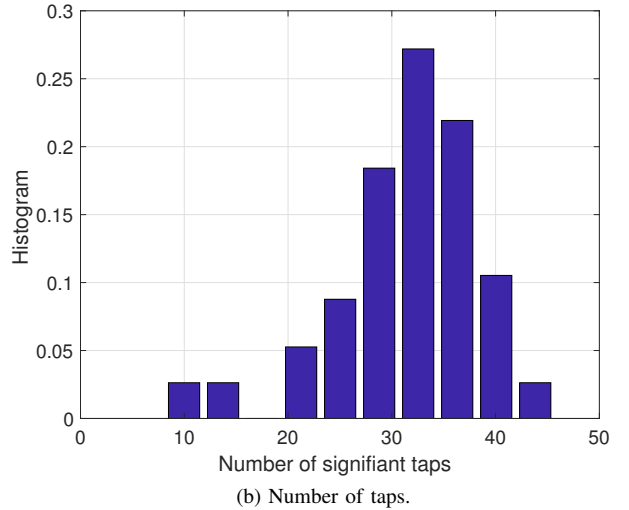
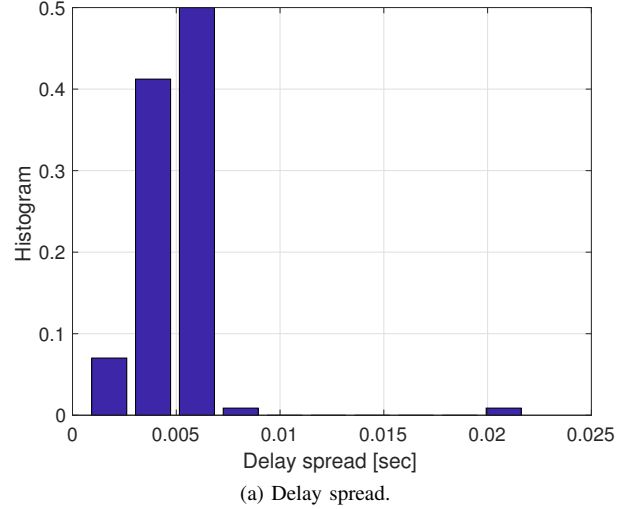


Fig. 3. Histogram of estimated features from a sea experiment.

we observe that the most significant differences are obtained for the number of taps and the delay spread, and that such differences for these features hold in a variety of experiments, as can be inferred from their very small confidence intervals.

Finally, the results confirm that the flexibility offered by the generalized Gaussian distribution in (1) is indeed required in practical settings. Fig. 3 shows the histogram of both the delay spread and the number of taps of a single time-varying channel measurement from our database. We observe that the shape of the distributions is different for each feature. Still, it is possible to model both distributions via the generalized Gaussian distribution (1), after a proper choice of the distribution's parameters.

VI. NUMERICAL RESULTS

We evaluate our cooperative authentication approach using realistic channel simulations obtained through the Bellhop framework [42], an established ray-tracing tool to simulate acoustic propagation under water. We set our simulations in the Bay Area of San Diego, CA, between the latitude/longitude

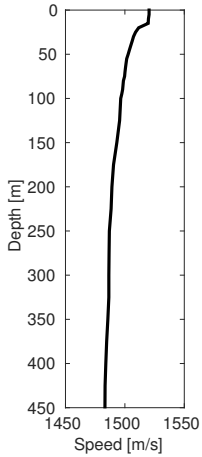


Fig. 4. Sound speed profile considered.

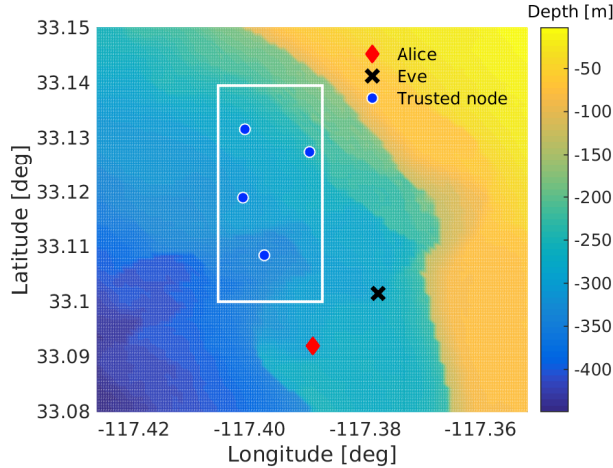


Fig. 5. Bathymetry map of the area, showing the location of Alice and the trusted node deployment area.

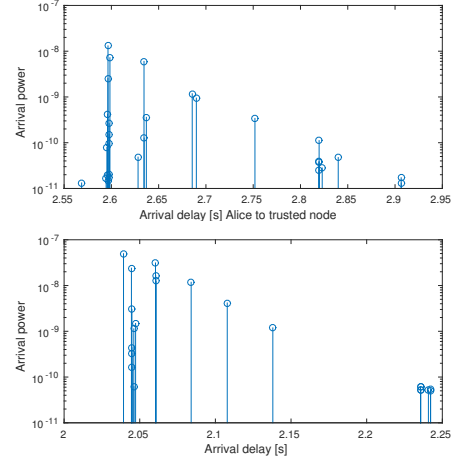


Fig. 6. Example of simulated channel impulse responses (top: Alice, bottom: Eve).

coordinates $[32.6^\circ, -117.8^\circ]$ and $[33.3^\circ, -117.2^\circ]$. The setting is characterized by a continental shelf zone with a quasi-flat bottom, of a depth between 50 and 100 m, followed by a ridge, which plunges to lower depths. Here we consider a portion of this area, whose bathymetry map is shown in Fig. 5. In this portion, the depth ranges from about 10 m in the top-right corner of the map, to about 450 m in the bottom-left corner. We assume that the bottom sediments are mostly sandy and that the sound speed profile is as shown in Fig. 4, which corresponds to an actual measurement taken during the summer season. Furthermore, we assume a flat ocean surface.

Fig. 5 also provides a view of our simulation setup. The locations of the legitimate transmitter (Alice) and the attacker (Eve) are shown as a red diamond and a black cross, respectively. The distance between the legitimate node and the attacker is about 1500 m. The trusted nodes are deployed within the area enclosed in the white frame, which has a size of about $2 \text{ km} \times 2 \text{ km}$ (notice that the scale is different on the x-axis and y-axis in Fig. 5). An example of the channel impulse responses estimated by Bellhop for this setup is shown in Fig. 6, where we depict the channel's power-delay profile from the legitimate node to the rightmost trusted node in Fig. 5 (top panel), and of the channel from the attacker to the same trusted node (bottom panel). Assuming a realistic transmission system with 10 kHz of bandwidth, the power-delay profiles have been filtered such that no two arrivals exist whose delays are less than $100 \mu\text{s}$ apart. The results of Fig. 6 show that the arrivals distribute and cluster differently over time, as expected after the analysis on real channel parameters in Section V-B.

We collect a Monte-Carlo set of 500 simulation runs. In each run, the location and depth of the trusted nodes are uniformly drawn at random, whereas the locations of the legitimate node and the attacker remain fixed. Each simulation run corresponds to the transmission of a total of six packets from the legitimate transmitter to all trusted nodes, and of one packet from the attacker, also directed to all trusted nodes. Each packet includes 100 symbols, out of which each trusted node produces 100 estimates of the channels' number of taps

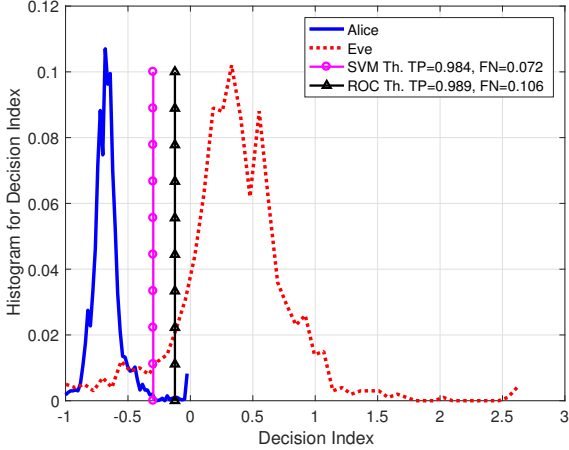
(19), RMS delay spread (22), and the smoothed received power (24). The difference among these estimates is rendered in the simulations by assuming that all nodes are moored, and that they oscillate around the mooring location. To achieve this, before a channel estimate is computed by Bellhop, the transmitter and the receiver are randomly displaced by up to a few meters from their nominal location.

A. Attack Strategy

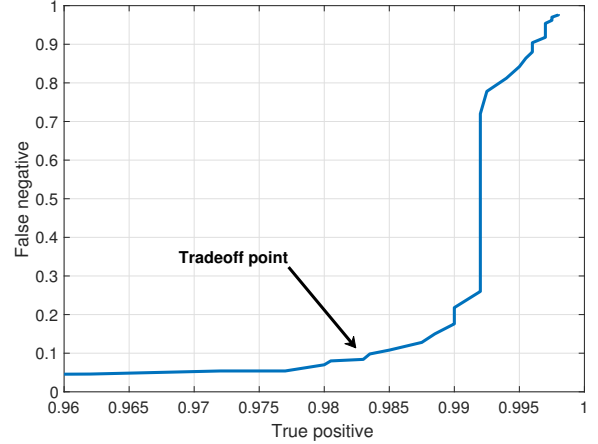
To implement the attacker model in Section III-B, we consider different attacker capabilities which, in turn, enable increasingly complex attack strategies. The most typical case is that of a straightforward impersonation attack, where the attacker tries to disguise himself as the transmitter by simply injecting packets into the network towards all trusted nodes. While this is a simple attack, it can still succeed if, e.g., the attacker is positioned close to the legitimate node. We model this *naïve* attack by using the Bellhop software [42] to estimate the channel impulse response from the legitimate node or the attacker to all of the trusted nodes.

A more powerful attack, referred to as *TN-1*, is enabled if the attacker can estimate the channel impulse response between the legitimate node and one of the trusted nodes, and can leverage an array of transducers in order to mimic this response. To compute the channel estimate, we assume the attacker knows the exact sound speed profile and the location of both legitimate and trusted nodes, but has an imperfect bathymetry map of the area. In this version, each sample is affected by both a constant offset Δz and random noise. The attacker runs the same acoustic propagation model provided by Bellhop to estimate the channel impulse response and then pre-processes its transmission, such that it will be received as having gone through the estimated legitimate node-trusted node channel.

An even more complex attack is obtained by assuming that the attacker can mimic the channel response between the legitimate node and more trusted nodes, ultimately all of them. This attack is referred to as *TN-x*. This makes it possible for



(a) Histogram of data, and results of the two types of decision schemes.



(b) ROC curve.

Fig. 7. Simulation results of decision index Ψ_ϕ from (5) for a naïve attacker. The obtained authentication accuracy is 97%.

the attacker to completely disguise itself as the legitimate node, as far as is allowed by the attacker’s capability to estimate the channels between legitimate and trusted nodes.

We stress that trying to fool a single trusted node in TN-1 requires several complex steps, including channel estimation, channel inversion and pre-coding, but may still be possible for an underwater attacker endowed with a large transceiver array and sufficient computational power. Instead, fooling multiple cluster nodes at the same time in TN- x , $x > 1$, would require the deployment of multiple, perfectly coordinated transceiver array elements at different locations in the network area. This is much less realistic in any practical scenario.

B. Determining the Threshold level

In order to make the authentication decision in (5), the decision threshold, λ , needs to be determined. Ideally, this threshold is set by finding the analytical relationship between the false alarm probability, the detection probability, and the threshold. Since, in our case, this analysis is extremely complex and also for the channel distribution model, we instead set λ statistically.

We offer two approaches. The first is to determine the receiver operating characteristic (ROC) curve by numerically evaluating the false-negative (FN) rate and the true-positive (TP) rate (*ROC test*). The second method is based on a support vector machine (SVM), namely an *SVM-test*, to classify the two hypotheses, based on the decision index. Both methods are based on dividing the simulation data into a *training* part and a *test* part. The threshold computation is performed only on the training data set, whereas the data analysis is performed only on the test set.

In the ROC test, we try a set of threshold values over the training data and draw the TP rate against the FN rate. We then determine a desirable working point that trades off between the values of these two metrics. In the SVM test, we avoid setting such a tradeoff, and instead seek the threshold that yields the best classification solution. To this end, we set a K-fold test to determine the classifier’s parameters, and train the SVM model

based on the training set. Classification is performed on the test set, and the threshold is determined based on the minimum decision index from all packets classified as belonging to the attacker.

C. Simulation Results

We first describe the simulation results for the naïve attacker, where the attacker transmits its packets directly, without any preprocessing. Fig. 7a shows the histogram of the decision index, normalized within the $[-1, 1]$ range, for 1,000 simulated test scenarios, together with the ROC test-based threshold and the SVM test-based threshold. The former was set based on the ROC curve in Fig. 7b, and we choose as a best practice (at least under the assumption that the channel does not vary significantly) the *knee* point in the ROC curve to yield a desired FN probability of 0.1 and a TP probability of 0.98. The SVM test-based threshold was obtained from a radial function basis (RBF) kernel SVM with a $K = 5$ -fold training procedure. The procedure achieved an excellent authentication accuracy of 97%. We observe that the decision index values for the legitimate packets (Alice) and the attacker’s packets (Eve) are well distinguished. Although they have been obtained through different procedures, the threshold based on the SVM test is close to the one based on the ROC test. However, the SVM-based threshold yields a slightly better performance (the same TP, but lower FN).

Next, we explore the performance of our authentication method against the more advanced attacker, which matches its transmitted signals, such that the attacker-trusted node channel is as close to the legitimate node-trusted node channel as the attacker’s capability to estimate this channel allows. Recall that this requires the attacker to accurately estimate the bathymetry as well as the location of the legitimate node and the trusted node. We recall that we favor the attacker by assuming that it possesses perfect knowledge of the legitimate nodes and the trusted nodes’ location, knowledge of the SSP and of the sediments on the bottom (as is necessary to run the Bellhop propagation model), and slightly erroneous knowledge

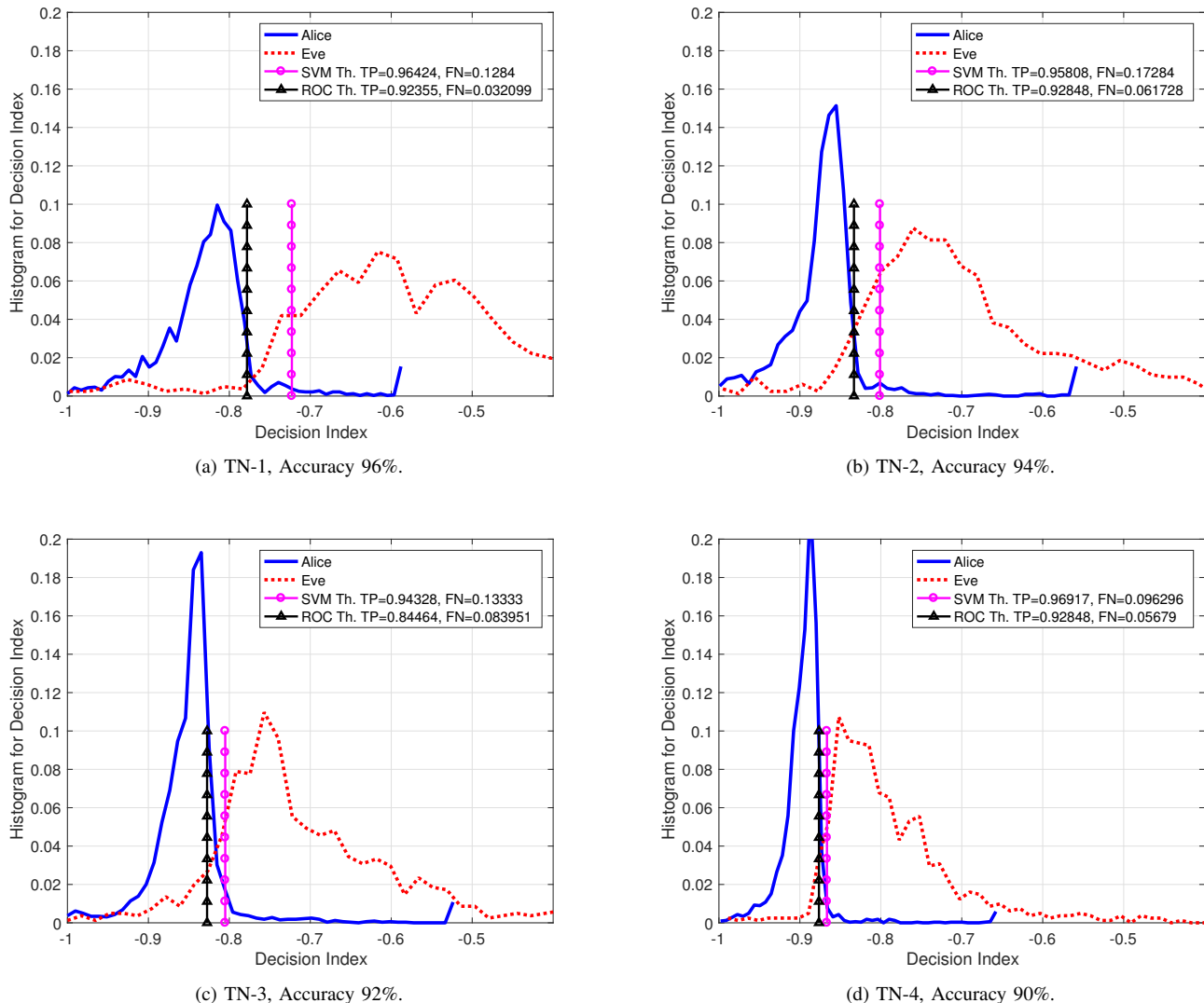


Fig. 8. Simulation results of decision index Ψ_ϕ from (5) for an advanced attacker.

of the bathymetry. Specifically, we assume that the attacker's bathymetry knowledge is affected by an offset amounting to about 5% of the area's maximum depth. Additionally, each bathymetry sample is affected by a random error of $\pm 0.5\%$ of the area's maximum depth.

We illustrate the authentication algorithm performance for the case where the attacker imitates the channel to a single trusted node (TN-1, Fig. 8a); to two trusted nodes (TN-2, Fig. 8b); to three trusted nodes (TN-3, Fig. 8c); and to all four trusted nodes (TN-4, Fig. 8d). Since the packets arrive almost simultaneously to all of the trusted nodes, the last three cases of TN-2, TN-3, and TN-4 are unfeasible without an advanced and large transmission array. Still, we give them to show the limitations of our authentication method. For all cases, we also give the ROC performance as obtained by the statistical approach and by the SVM approach. In each figure's caption, we list the accuracy obtained by the SVM approach. As expected, comparing the histograms of the four cases and those in Fig. 7a, we observe that the two decision index

classes become less distinct, the better the attacker imitates the channel to more trusted nodes. However, the results show that, even for this advanced attacker, authentication performance is acceptable with a classification accuracy of 96% for (the more feasible case) TN-1.

VII. SEA EXPERIMENT

In this section, we describe the setup and results obtained from a sea experiment conducted in May 2017 near the Hadera coal pier in northern Israel. The experiment's goal was to demonstrate the effectiveness of our authentication method under real sea conditions. In particular, compared to our Bellhop simulations whose time-variation was obtained through small simulated movements, we wanted to test performance for a realistic time-varying underwater acoustic channel.

A. Setup

The sea experiment set-up is illustrated in Fig. 9. The experiment included five nodes — two transmitters (station

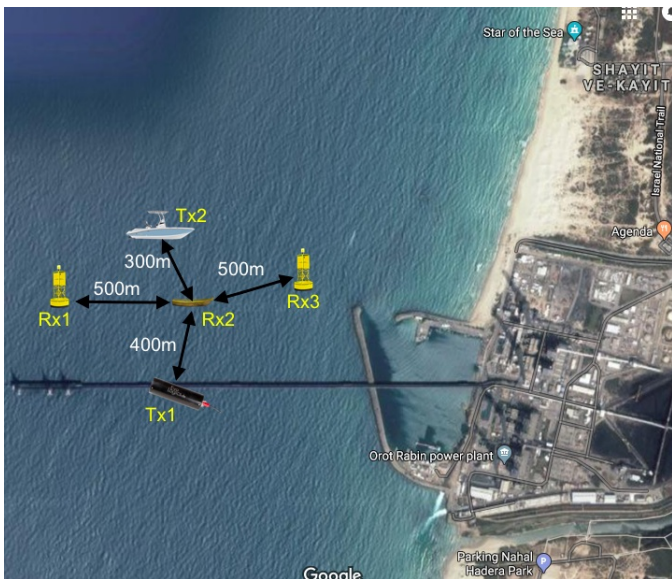


Fig. 9. An illustration of the sea experiment's setup.

Tx1 on a long coal pier that stretches 2 km into the sea, and station Tx2 on the larger boat), and three receivers (station Rx2 on the smaller boat, and stations Rx1 and Rx3 on floating buoys). The transmitters were placed roughly 1,000 m apart, and the three receivers were deployed in a line with spacing of roughly 500 m. The distances between the boat transmitter and the pier transmitter to the receiver on the smaller boat were roughly 200 m and 400 m, respectively. The water depth was about 25 m, and the modems and receivers were deployed at a depth of about 10 m. During the experiment, the sea was rough, with a sea level of 3 and waves rising to over 1.5 m. We note that due to the pier's thick stone columns, the transmissions of Tx1 were not received by Rx1.

The two transmitters were based on the EvoLogics software defined S2C R 7/17 modems, and transmitted short chirp-modulated packets, each with 100 symbols in the frequency band between 7 kHz and 17 kHz of duration 0.1 s. Transmissions were made with high power of roughly 175 dB re $1\mu\text{Pa}@1\text{m}$. The receivers were based on a Cetacean CR1 hydrophone, and recorded continuously throughout the experiment. We tested two scenarios. In Scenario I, the boat transmitter was the legitimate node and the pier transmitter was the attacker, and vice versa in Scenario II. In both cases, the legitimate node sent 7 packets, and the attacker sent two packets.

The recorded data was processed offline to evaluate the channel's characteristics for each transmitter-receiver link. Since the transmitted signals were wideband (relative to the carrier frequency) and transmitted with high SNR, channel estimates were obtained by processing the received signals through a matched filter. Based on our preliminary analysis in Section V, for the purpose of authentication, for each symbol we evaluated the delay spread (22), the number of taps (19), and the smoothed received level (24). Our results show that, in the case of this experiment, also including the average tap's power (20) was beneficial due to the different attenuation.

B. Results

We start by showing the estimated values of the four authentication parameters from the sea experiment. In Fig. 10a, we show the average per-packet delay spread values from the three receivers. We observe that packets 8 and 9 from the attacker (Eve) are well distinguished from packets 1-7 from the legitimate node (Al). A similar effect is shown in Figs. 10b and 10c for the average per-packet number of taps and the average channel's tap power. Instead, Fig. 10d shows the per-packet smoothed received power level, and we observe that in Rx1 there is no difference between the two packet types. While this may have caused some performance degradation, since in Rx2 the average smoothed received level values of the attacker's packets are very different than those of the legitimate node's packets, the effect on performance is limited.

In regard to the authentication procedure applied in the sea experiment, in Fig. 11 we show the normalized values for the decision index Ψ_ϕ for the two tested scenarios as a function of the packet index. We observe that the seven packets from the legitimate transmitter are roughly similar to all packets from the legitimate transmitter, and are well distinguished from both of the attacker's packets. We also show the threshold level obtained from the simulations for the worst case scenario of an advanced attacker TN-1 (see Section VI-B). Comparing the threshold values, a correct decision is made for both types of packets. We therefore conclude that our method succeeded in detecting the attacker's packets in a real sea environment.

VIII. CONCLUSIONS

The increasing use of wireless techniques underwater has increased the need to secure underwater communications. In particular, since most of the available acoustic modems do not naturally include encryption, an intruder may introduce fake messages into the system. In this paper, we presented a new cooperative message authentication method for use with an underwater acoustic network. Our method leverages the strong spatial dependency of the underwater acoustic channel to perform authentication based on the computation of a decision index, calculated by a set of trusted nodes as a maximum likelihood test over the estimated distribution of some key underwater acoustic channel's coefficients. While the trusted nodes act in a distributed fashion, the final decision is performed by a sink node without the need to communicate the outcome to the trusted nodes. We discussed the choice of channel parameters for message authentication, as well as the detailed steps of our scheme. Extensive model-based numerical simulations, as well as demonstrations in two sea experiments prove the effectiveness of our scheme. Further work will extend our approach to intruder detection.

APPENDIX

In this Appendix, we focus on a single channel feature i and a single node n . We therefore drop the indices i, n from all notation. To estimate $\theta(p)$, we use the iterative expectation maximization (EM) algorithm [37] to update the estimate of θ iteratively. Denote $\hat{\theta}(p+1) = (\hat{\omega}^m(p+1), \hat{k}^m(p+1))$ as the estimate obtained at the end of iteration p .

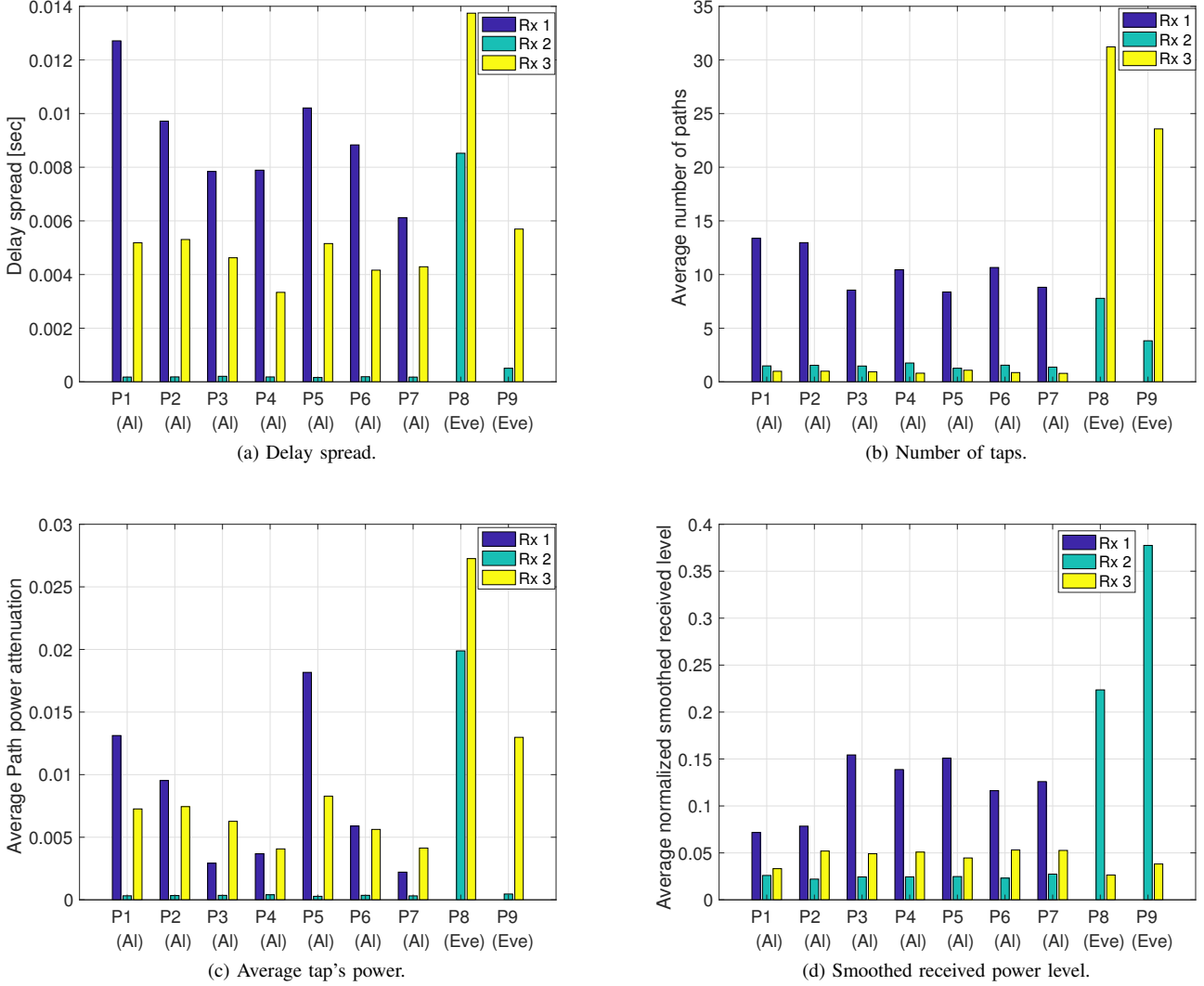


Fig. 10. Average per-packet evaluations of the authentication parameters from the sea experiment.

With the constraint that all estimates within one of the previously received packets $f = 1, \dots, \phi$ must be assigned to the same hypothesis ($m = 0, 1$), we define $y(f) \in \{1, 2\}$ as the label assigned to packet f , to be estimated. Let $\mathcal{Y}(\phi) = \{y(t), t \in \mathcal{T}_f, f \leq \phi\}$ be the set of estimated labels for feature i at node n up to packet ϕ , and $\mathbf{Y}(f) = \{y(t), t \in \mathcal{T}_f\}$. In addition, let $\bar{\mathcal{X}}(f)$ be a subset of $\mathcal{X}(\phi)$ including only those measurements x that are obtained from packet $f = \{0, \dots, \phi\}$. The expectation of the log-likelihood function with respect to the conditional distribution of θ at iteration p , given $\mathcal{X}(\phi)$ and the estimate of the previous iteration $\tilde{\theta}(p)$, is

$$\begin{aligned}
 L(\theta|\tilde{\theta}(p)) &= \mathbb{E} \left[\ln(\mathbb{P}(\mathcal{X}(\phi), \mathcal{Y}(\phi)|\theta)) | \bar{\mathcal{X}}(\phi), \tilde{\theta}(p) \right] \\
 &= \sum_{m=1}^2 \sum_{f=1}^F \mathbb{P}(y(f) = m | \mathbf{X}(f), \tilde{\theta}(p)) \\
 &\quad \times \left[\ln \tilde{k}^m(p) + \sum_{x \in \bar{\mathcal{X}}(f)} \ln p_{x|\omega^m}(x | \tilde{\omega}^m(p)) \right], \quad (27)
 \end{aligned}$$

where the posterior is

$$\begin{aligned}
 \mathbb{P}(y(f) = m | \bar{\mathcal{X}}(f), \tilde{\theta}(p)) &= \frac{\tilde{k}^m(p) \mathbb{P}(\mathcal{X}(f) | \tilde{\omega}^m(p))}{\mathbb{P}(\bar{\mathcal{X}}(f) | \tilde{\theta}(p))} \\
 &= \frac{\tilde{k}^m(p) \prod_{x \in \bar{\mathcal{X}}(f)} p_{x|\omega^m}(x | \tilde{\omega}^m(p))}{\sum_{j=1}^2 \tilde{k}^j(p) \prod_{x \in \bar{\mathcal{X}}(f)} p_{x|\omega^m}(x | \tilde{\omega}^j(p))}, \quad (28)
 \end{aligned}$$

and $\ln x = \log_e x$ is the natural logarithm of x .

To obtain $\tilde{k}^m(p+1)$, we maximize the second term of (27) to yield (see details in [37]),

$$\tilde{k}^m(p+1) = \frac{1}{\phi} \sum_{f=1}^{\phi} \mathbb{P}(y(f) = m | \bar{\mathcal{X}}(f), \tilde{\theta}(p)). \quad (29)$$

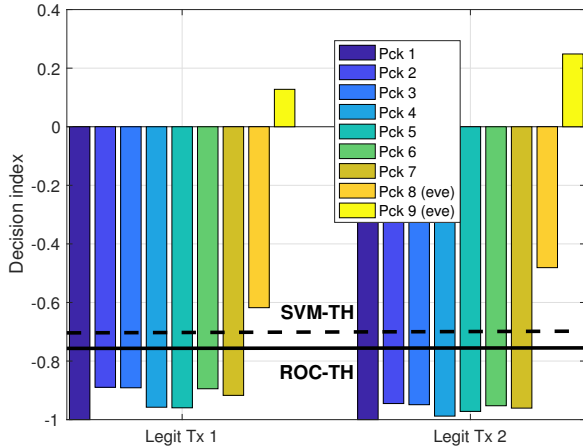


Fig. 11. Normalized authentication decision index (14) from a sea experiment. Two scenarios are shown for seven legitimate packets and two attacker's packets. The SVM- and ROC-based thresholds for TN-1 from the simulations are also shown.

To obtain $\tilde{\omega}^m(p+1)$, we maximize the first term of (27)

$$\begin{aligned}
& \sum_{f=1}^{\phi} \mathbb{P}(y(f) = m | \tilde{\mathcal{X}}(f), \tilde{\theta}(p)) \cdot \ln \mathbb{P}(\tilde{\mathcal{X}}(f) | \tilde{\omega}^m(p+1)) = \\
& = \sum_{f=1}^{\phi} \mathbb{P}(y(f) = m | \tilde{\mathcal{X}}(f), \tilde{\theta}(p)) \\
& \times \sum_{x \in \tilde{\mathcal{X}}(f)} \left[\ln \tilde{\beta}^m(p+1) - \ln(2\tilde{\sigma}^m(p+1)) \right. \\
& \quad \left. - \ln \Gamma\left(\frac{1}{\tilde{\beta}^m(p+1)}\right) - \left(\frac{|x - \tilde{\mu}^m(p+1)|}{\tilde{\sigma}^m(p+1)}\right)^{\tilde{\beta}^m(p+1)} \right].
\end{aligned} \quad (30)$$

The result is obtained numerically by solving for $\tilde{\mu}^m(p+1)$,

$$\begin{aligned}
0 & = \sum_{f=1}^{\phi} \mathbb{P}(y(f) = m | \tilde{\mathcal{X}}(f), \tilde{\theta}(p)) \\
& \times \sum_{x \in \tilde{\mathcal{X}}(f)} (x - \tilde{\mu}^m(p+1)) (|x - \tilde{\mu}^m(p+1)|)^{\tilde{\beta}^m(p)-2}, \quad (31)
\end{aligned}$$

then for $\tilde{\sigma}^m(p+1)$,

$$\begin{aligned}
0 & = \sum_{f=1}^{\phi} \mathbb{P}(y(f) = m | \tilde{\mathcal{X}}(f), \tilde{\theta}(p)) \sum_{x \in \tilde{\mathcal{X}}(f)} \left(-\frac{1}{\tilde{\sigma}^m(p+1)} \right. \\
& \quad \left. + \frac{\tilde{\beta}^m(p) (|x - \tilde{\mu}^m(p+1)|)^{\tilde{\beta}^m(p)-1}}{\tilde{\sigma}^m(p+1)} \right), \quad (32)
\end{aligned}$$

and finally for $\tilde{\beta}^m(p+1)$,

$$\begin{aligned}
0 & = \sum_{f=1}^{\phi} \mathbb{P}(y(f) = m | \tilde{\mathcal{X}}(f), \theta(p)) \\
& \times \left[\frac{1}{\tilde{\beta}^m(p+1)} + \frac{d\left(\frac{1}{\tilde{\beta}^m(p+1)}\right)}{(\tilde{\beta}^m(p+1))^2} \right. \\
& \quad \left. + \sum_{x \in \tilde{\mathcal{X}}(f)} \ln\left(\frac{|x - \tilde{\mu}^m(p+1)|}{\tilde{\sigma}^m(p+1)}\right) \times \right. \\
& \quad \left. \times \left(\frac{|x - \tilde{\mu}^m(p+1)|}{\tilde{\sigma}^m(p+1)}\right)^{\tilde{\beta}^m(p+1)} \right], \quad (33)
\end{aligned}$$

where $d(\cdot)$ is the digamma function.

After the convergences of the EM procedure, we calculate the posterior $\mathbb{P}(y(f) = m | \tilde{\mathcal{X}}(f), \tilde{\theta}(p+1))$. We use this posterior as a soft decision parameter to identify packet f with set m . To consistently identify sets $m = \{0, 1\}$ between the different trusted nodes, for the first received packet, we determine $m = 1$ as the set m that yields the highest posterior.

To initiate the EM, we use the k-means algorithm [37] to cluster $\mathcal{X}(\phi)$ into two groups. For each group m , we statistically evaluate $\tilde{\omega}^m(0)$ using the following statistics for distribution (1)

$$\mathbb{E}[\mathcal{X}(\phi)] = \tilde{\mu}^m(0) \quad (34a)$$

$$\mathbb{E}[|\mathcal{X}(\phi) - \tilde{\mu}^m(0)|^2] = \frac{\tilde{\sigma}^{2m}(0) \Gamma\left(\frac{3}{\tilde{\beta}^m(0)}\right)}{\Gamma\left(\frac{1}{\tilde{\beta}^m(0)}\right)} \quad (34b)$$

$$\begin{aligned}
\text{Kurtosis} & = \frac{\mathbb{E}[(\mathcal{X}(\phi) - \tilde{\mu}^m(0))^2]}{(\mathbb{E}[|\mathcal{X}(\phi) - \tilde{\mu}^m(0)|^2])^2} = \\
& = \frac{\Gamma\left(\frac{5}{\tilde{\beta}^m(0)}\right) \Gamma\left(\frac{1}{\tilde{\beta}^m(0)}\right)}{\Gamma\left(\frac{3}{\tilde{\beta}^m(0)}\right)^2} - 3, \quad (34c)
\end{aligned}$$

where the above mean, variance, and Kurtosis are calculated using standard methods. Similarly, the prior $\tilde{k}^m(0)$ is estimated as the fraction of the elements of $\mathcal{X}(\phi)$, which is part of the m th cluster after the k-means algorithm.

REFERENCES

- [1] J. Potter, J. Alves, D. Green, G. Zappa, I. Nissen, and K. McCoy, "The janus underwater communications standard," in *2014 Underwater Communications and Networking (UComms)*, Sept 2014, pp. 1–4.
- [2] E. Souza, H. C. Wong, I. Cunha, . Cunha, L. F. M. Vieira, and L. B. Oliveira, "End-to-end authentication in underwater sensor networks," in *Proc. IEEE ISCC*, Split, Croatia, Jul. 2013.
- [3] G. Han, J. Jiang, N. Sun, and L. Shu, "Secure communication for underwater acoustic sensor networks," *IEEE Transactions on Mobile Computing*, vol. 53, no. 8, pp. 54–60, Aug. 2015.
- [4] H. Kulhandjian, T. Melodia, and D. Koutsonikolas, "Securing underwater acoustic communications through analog network coding," in *Proc. IEEE SECON*, Singapore, Jun. 2014.
- [5] L. Xiao, Q. Li, T. Chen, E. Cheng, and H. Dai, "Jamming games in underwater sensor networks with reinforcement learning," in *Proc. IEEE GLOBECOM*, San Diego, CA, Dec. 2015.
- [6] G. Dini and A. Lo Duca, "A secure communication suite for underwater acoustic sensor networks," *MDPI Sensors*, vol. 12, pp. 15 133–15 158, 2012. [Online]. Available: <http://dx.doi.org/10.3390/s121115133>
- [7] Y. Liu, J. Jing, and J. Yang, "Secure underwater acoustic communication based on a robust key generation scheme," in *Proc. ICSP*, Beijing, China, Oct. 2008.

- [8] G. Leus and P. A. van Walree, "Multiband OFDM for covert acoustic communications," *IEEE Journal on Selected Areas in Communications*, vol. 26, no. 9, pp. 1662–1673, Dec. 2008.
- [9] C. Lal, R. Petroccia, M. Conti, and J. Alves, "Secure underwater acoustic networks: Current and future research directions," in *Proc. IEEE UComms*, Lerici, Italy, Aug. 2016.
- [10] M. Zuba, Z. Shi, Z. Peng, and J.-H. Cui, "Launching denial-of-service jamming attacks in underwater sensor networks," in *Proc. ACM WUWNet*, Seattle, Washington, Dec. 2011.
- [11] M. Zuba, Z. Shi, Z. Peng, J.-H. Cui, and S. Zhou, "Vulnerabilities of underwater acoustic networks to denial-of-service jamming attacks," *Wiley Security and Communication Networks*, vol. 8, no. 16, pp. 2635–2645, Nov. 2015.
- [12] G. Caparra, M. Centenaro, N. Laurenti, S. Tomasin, and L. Vangelista, "Energy-based anchor node selection for iot physical layer authentication," in *Proc. IEEE ICC*, Kuala Lumpur, Malaysia, May 2016.
- [13] D. Torrieri, *Principles of spread-spectrum communication systems*. New York: Springer, 2011.
- [14] G. Danezis, *Covert Communications Despite Traffic Data Retention*. Springer Berlin Heidelberg, 2011, pp. 198–214.
- [15] M. Li, S. N. Batalama, D. A. Pados, T. Melodia, M. J. Medley, and J. D. Matyjas, "Cognitive code-division links with blind primary-system identification," *IEEE Trans. Wireless Commun.*, vol. 10, no. 11, pp. 3743–753, Nov. 2011.
- [16] R. Diamant, L. Lampe, and E. Gamroth, "Bounds for low probability of detection for underwater acoustic communication," *IEEE Journal of Oceanic Engineering*, vol. 42, no. 1, pp. 143–155, Jan 2017.
- [17] E. Jorswieck, S. Tomasin, and A. Sezgin, "Broadcasting into the uncertainty: Authentication and confidentiality by physical-layer processing," *Proceedings of the IEEE*, vol. 103, no. 10, pp. 1702–1724, Oct 2015.
- [18] T. Daniels, M. Mina, and S. Russell, "A signal fingerprinting paradigm for general physical layer and sensor network security and assurance," in *Proc. IEEE First Int. Conf. on Security and Privacy for Emerging Areas in Commun. Networks (SECURECOMM)*, Athens (Greece), Sep. 2005, pp. 1–3.
- [19] D. Faria and D. Cheriton, "Detecting identity-based attacks in wireless networks using signalprints," in *Proc. ACM Workshop on Wireless Security (WiSe)*, Los Angeles (CA), Sep. 2006, pp. 43–52.
- [20] M. Demirbas and Y. Song, "An RSSI-based scheme for sybil attack detection in wireless sensor networks," in *Proc. IEEE Int. Symp. on a World of Wireless, Mobile and Multimedia Networks (WoWMoM)*, Buffalo (NY), Jun. 2006.
- [21] Y. Chen, W. Trappe, and R. Martin, "Detecting and localizing wireless spoofing attacks," in *Proc. IEEE Conf. on Sensor, Mesh and Ad Hoc Commun. and Networks (SECON)*, San Diego (CA), Jun. 2007, pp. 193–202.
- [22] L. Xiao, L. Greenstein, N. Mandayam, and W. Trappe, "Fingerprints in the ether: using the physical layer for wireless authentication," in *Proc. IEEE Int. Conf. on Commun. (ICC)*, Glasgow (UK), Jun. 2007.
- [23] —, "A physical-layer technique to enhance authentication for mobile terminals," in *Proc. IEEE Int. Conf. on Commun. (ICC)*, Beijing (China), May 2008.
- [24] L. Xiao, L. J. Greenstein, N. Mandayam, and W. Trappe, "Channel-based spoofing detection in frequency-selective Rayleigh channels," *IEEE Trans. Wireless Commun.*, vol. 8, no. 12, pp. 5948–5956, Dec. 2009.
- [25] L. Xiao, A. Reznik, W. Trappe, Y. S. C. Ye, and L. Greenstein, "PHY-authentication protocol for spoofing detection in wireless networks," in *Proc. IEEE Global Telecommun. Conf. (GLOBECOM)*, Miami (FL), Dec. 2010, pp. 1–6.
- [26] F. He, W. Wang, and H. Man, "REAM: rake receiver enhanced authentication method," in *Proc. IEEE Military Communications Conference (MILCOM)*, Oct. 2010, pp. 2205–2210.
- [27] F. He, H. Man, D. Kivanc, and B. McNair, "EPSON: enhanced physical security in OFDM networks," in *Proc. IEEE Int. Conf. on Commun. (ICC)*, 2009, pp. 1–5.
- [28] J. K. Tugnait, "Wireless user authentication via comparison of power spectral densities," *IEEE Journal on Selected Areas in Communications*, vol. 31, no. 9, pp. 1791–1802, September 2013.
- [29] A. Mahmood, W. Aman, M. O. Iqbal, M. M. U. Rahman, and Q. H. Abbasi, "Channel impulse response-based distributed physical layer authentication," in *2017 IEEE 85th Vehicular Technology Conference (VTC Spring)*, June 2017, pp. 1–5.
- [30] L. Xiao, X. Wan, and Z. Han, "Phy-layer authentication with multiple landmarks with reduced overhead," *IEEE Transactions on Wireless Communications*, vol. PP, no. 99, pp. 1–1, 2017.
- [31] K. G. Kebkal, O. Kebkal, and R. Petroccia, "Assessment of underwater acoustic channel during payload data exchange with hydro-acoustic modems of the S2C series," in *MTS/IEEE OCEANS*, Genova, Italy, May 2015.
- [32] M. Stojanovic and J. Preisig, "Underwater acoustic communication channels: Propagation models and statistical characterization," *IEEE Communications Magazine*, vol. 47, no. 1, pp. 84–89, 2009.
- [33] B. Katsnelson, V. Petnikov, and J. Lynch, *Fundamentals of shallow water acoustics*. Springer Science & Business Media, 2012, ch. 3, 4.
- [34] M. Ainslie, P. Dahl, C. de Jong, and R. Laws, "Practical spreading laws: The snakes and ladders of shallow water acoustics," in *Proc. UA*, Rhodes, Greece, Jun. 2014.
- [35] R. Urick, *Sound propagation in the sea*. Peninsula Publishing Newport Beach, 1982.
- [36] M. Novey, T. Adali, and A. Roy, "A complex generalized Gaussian distribution: Characterization, generation, and estimation," *IEEE Trans. Signal Process.*, vol. 58, pp. 1427–1433, Mar. 2010.
- [37] S. Kay, *Fundamentals of Statistical Signal Processing: Estimation Theory*. Englewood Cliffs, NJ: Prentice-Hall, 1993.
- [38] D. Shepard, "A two-dimensional interpolation function for irregularly spaced data," *Assoc. of Computing Machinery*, vol. 23, pp. 517–524, 1968.
- [39] R. Diamant, "Closed form analysis of the normalized matched filter with a test case for detection of underwater acoustic signals," *IEEE Access*, vol. 4, pp. 8225–8235, 2016.
- [40] R. Diamant and L. Cherev, "Emulation system for underwater acoustic channel," in *International Undersea Defence Technology Europe conference (UDT)*, vol. 2, Amsterdam, the Netherlands, Jun. 2005, pp. 1043–1046.
- [41] R. Jain, W. Hawe, and D. Chiu, "A quantitative measure of fairness and discrimination for resource allocation in shared computer systems," Eastern Research Lab, Tech. Rep. DEC-TR-301, 1984.
- [42] M. Porter *et al.*, "Bellhop code," Last time accessed: Nov. 2015. [Online]. Available: <http://oalib.hlsresearch.com/Rays/index.html>